Charge-transfer chemistry of two corticosteroids used adjunctively to treat COVID-19. Part I: Complexation of hydrocortisone and dexamethasone donors with DDQ acceptor in five organic solvents

Abdel Majid A. Adam [a],*, Hosam A. Saad: [a], Moamen S. Refat [a], Mohamed S. Hegab [b]

[a] Department of Chemistry, College of Science, Taif University, P.O. Box 11099, Taif 21944, Saudi Arabia
[b] Deanship of Supportive Studies (D.S.S.), Taif University, P.O. Box 11099, Taif 21944, Saudi Arabia

ABSTRACT

COVID-19 is the disease caused by a novel coronavirus (CoV) named the severe acute respiratory syndrome coronavirus 2 (termed SARS coronavirus 2 or SARS-CoV-2). Since the first case reported in December 2019, infections caused by this novel virus have led to a continuous global pandemic that has placed an unprecedented burden on health, economic, and social systems worldwide. In response, multiple therapeutic options have been developed to stop this pandemic. One of these options is based on traditional corticosteroids, however, chemical modifications to enhance their efficacy remain largely unexplored. Obtaining additional insight into the chemical and physical properties of pharmacologically effective drugs used to combat COVID-19 will help physicians and researchers alike to improve current treatments and vaccines (i.e., Pfizer-BioNTech, AstraZeneca, Moderna, Janssen). Herein, we examined the charge-transfer properties of two corticosteroids used as adjunctive therapies in the treatment of COVID-19, hydrocortisone and dexamethasone, as donors with 2,3-dichloro-5,6-dicyano-p-benzoquinone as an acceptor in various solvents. We found that the examined donors reacted strongly with the acceptor in CH_2Cl_2 and $CHCl_3$ solvents to create stable compounds with novel clinical potential.

© 2022 Elsevier B.V. All rights reserved.

1. Introduction

Since the influenza outbreak of 1918, the COVID-19 outbreak has become the biggest worldwide public health crisis. As of November 22, 2021, COVID-19 has infected more than 258 million people and caused over 5 million casualties worldwide [1–7]. Corticosteroids are a class of chemicals that includes mineralocorticoids, glucocorticoids, and steroid hormones. They have been used clinically as immunomodulatory and anti-inflammatory drugs for more than 70 years to treat oral infections, acute respiratory distress syndrome, and inflammatory diseases [8–14]. Two of the corticosteroids most widely used worldwide as adjunctive therapies in the treatment of COVID-19 are hydrocortisone and dexamethasone. Hydrocortisone (Fig. 1a) (11β,17α,21-trihydroxy pregn-4-ene-3,20-dione) (abbreviated here as HC) is a steroidal anti-inflammatory drug and anti-allergic glucocorticoid commonly used in the treatment of inflammation and severe skin allergies [15,16].

Dexamethasone (Fig. 1b) (9α-fluoro-16α-methyl-11β,17α,21-trihydroxy-1,4-pregnadiene-3,20-dione) (abbreviated here as DM) is a synthetic glucocorticosteroid well known for its potent anti-inflammatory effects, which are 16 times more potent than prednisolone and up to 25–50 times more potent than hydrocortisone [17–19].

Reactions that involve the transfer of an electronically charged particle from an electron-rich donor (D) molecule to an electron-deficient acceptor (A) molecule (D → A) are known as charge transfer (CT) complexations or donor–acceptor interactions [20–27]. The unique physical, biological, chemical properties of the products resulting from CT interactions have gained the attention of researchers in both basic (physics, chemistry, biochemistry, biology) and applied (engineering, material science, industry, technology, pharmacology, medicine) sciences [21,28–81].

In the past 10 years, we focused on the investigation of the CT interaction of numerous vital and biological active molecules with different kinds of acceptors [82–110]. Now, we seek to explore the CT complexation of two anti-inflammatory glucocorticosteroid compounds, hydrocortisone (HC) and dexamethasone (DM), currently used as adjunctive therapeutics in the treatment of COVID-19 in a series of related publications. The purpose of this
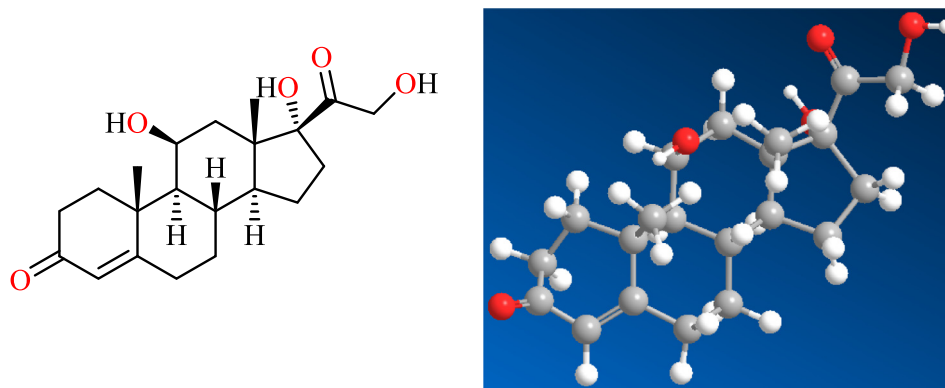
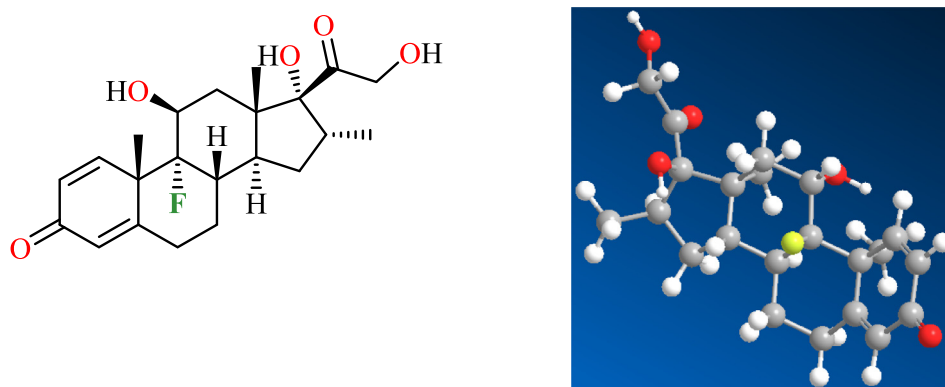**Fig. 1a.** Chemical structure of the HC donor.

Fig. 1b. Chemical structure of the DM donor.

part of work (Part I) was to determine the CT complexation behavior of the HC and DM molecules when complexed with the 2,3-dichloro-5,6-dicyano-p-benzoquinone (commonly termed as DDQ) acceptor (Fig. 2) in five different organic solvents namely methanol (MeOH; S1), ethanol (EtOH; S2), acetonitrile (MeCN; S3), dichloromethane (CH$_2$Cl$_2$; S4), and trichloromethane (CHCl$_3$; S5).

2. Experimental details

2.1. Chemicals

The investigated corticosteroids, hydrocortisone (HC) (362.46 g mol^{-1}; C$_{21}$H$_{30}$O$_5$; purity $\geq$ 98% HPLC) and dexametha-

Fig. 2. Chemical structure of the DDQ acceptor.

sone (DM) (392.46 g mol^{-1}; C$_{22}$H$_{29}$FO$_5$; purity $\geq$ 99% HPLC), were supplied by the Sigma–Aldrich (USA). The examined acceptor is 2,3-dichloro-5,6-dicyano-p-benzoquinone (commonly termed as DDQ) (C$_8$Cl$_2$N$_2$O$_2$; 227.0 g mol^{-1}; purity 98%) was obtained from Merck KGaA (Germany). The spectroscopic-grade solvents methanol (S1) (MeOH), ethanol (S2) (EtOH), acetonitrile (S3) (MeCN), dichloromethane (S4) (CH$_2$Cl$_2$), and trichloromethane (S5) (CHCl$_3$) were obtained from Fluka (Lausanne, Switzerland).

2.2. Spectrophotometric analysis

2.2.1. UV/Visible spectrophotometry

A Cary 7000 UV–Vis-NIR Spectrophotometer [Agilent Technologies Australia, Mulgrave, VICTORIA, Australia] was utilized to record the UV/Vis absorption spectra of the HC–DDQ and DM–DDQ system in each solvent (S1, S2, S3, S4, and S5). The spectra were scanned in the region of 200–800 nm at room temperature. After preparing standard solutions of HC, DM, and DDQ (5 × 10^{-4} M) in a specific solvent (S1, S2, S3, S4, or S5), 1 mL of the HC standard solution was mixed with 1 mL of the DDQ standard solution, then brought to 5 mL with the appropriate solvent to generate the HC–DDQ complex. The DM–DDQ complex was generated by adding 1 mL of the DM standard solution to 1 mL of the DDQ standard solution and bringing the volume of the mixture to 5 mL with the appropriate solvent. The UV/Vis spectra of the two soluble CT complexes (HC–DDQ and DM–DDQ) were scanned along with the corresponding free components. These spectra will help to characterize the CT phenomena and identify the λ_{CT} corresponding to the characteristic CT band for each complex.
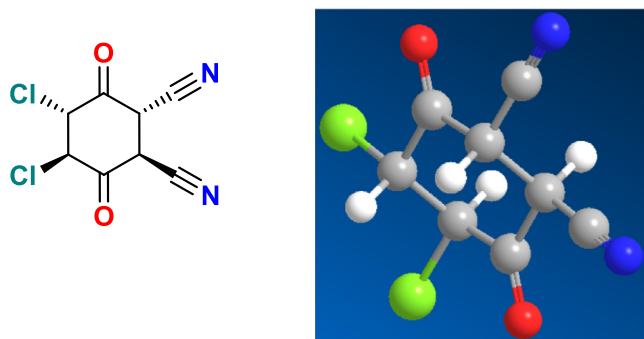
2.2.2. Fourier-Transform Infrared (FT–IR) spectrophotometry

An ALPHA Bruker Fourier-Transform Infrared Spectrometer [Bruker Optik GmbH; Ettlingen, Germany] was utilized to obtain the FT-IR absorption spectra of the solid CT complexes in each solvent in the region 4000–400 cm^{-1} at room temperature. After preparing a concentrated solution of HC, DM, and DDQ (two portions) by dissolving 2 mmol of each component in 20 mL of the appropriate solvent (S1, S2, S3, S4, or S5), these concentrated solutions were well-stirred, then mixed together (HC with DDQ and DM with DDQ; 1:1 M ratio). To harvest the solid CT complexes (HC–DDQ and DM–DDQ in each solvent) by slow evaporation, the mixed solutions were left overnight and the formed colored precipitates were removed from the solution by filtration. The collected HC–DDQ and DM–DDQ solid products were purified by washing three times with a small amount of the appropriate solvent and finally, air-dried. The ten purified, dried products were scanned by the IR instrument and plotted in transmission mode.

2.3. Elemental composition

The elemental compositions of the donors (HC and DM) with the DDQ acceptor were determined by collecting the carbon, nitrogen, and hydrogen contents (%) for each CT complex prepared in each solvent (S1, S2, S3, S4, and S5) using a Perkin-Elmer 2400 Series II CHNS Microanalyzer (PerkinElmer Inc., Waltham, MA, USA).

2.4. Stoichiometry of the HC–DDQ and DM–DDQ interaction

Generally, two methods based on the UV/Vis absorption spectra are applied to obtain the stochiometric reaction of the CT complexation, the spectrophotometric titration method and Job's continuous variation method. The HC and DM stoichiometric interactions with the DDQ acceptor were determined in each solvent (S1, S2, S3, S4, or S5) using both methods.

3. Results and discussion

3.1. Ultraviolet–visible (UV/Vis) characteristics

3.1.1. Donors and acceptor

The donors (HC and DM) are soluble in the S1 and S2 solvents; for the other solvents (S3, S4, and S5), slight heat is required to solubilize the corticosteroids used in the present study. All of the resulting solutions were colorless. In contrast, the DDQ acceptor's solubility and the resultant solutions varied according to the solvent. As with the two donors, the DDQ molecule was easily dissolved in the S1 and S2 solvents and, with gently heating, in the
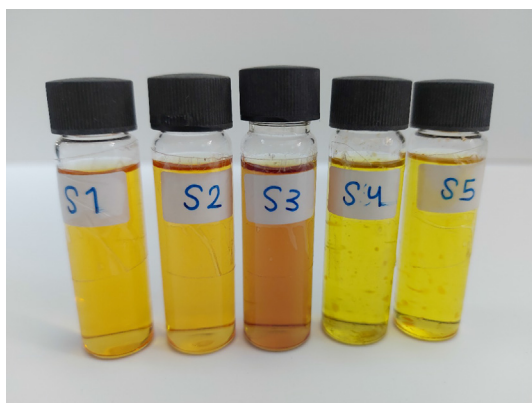
other three solvents. The resultant solutions in all of the solvents were colored as indicated in Fig. 3. Fig. 4 contains the UV/Vis spectra of the DDQ in each solvent (S1, S2, S3, S4, and S5). Its absorption characteristics depend on the solvent type and can be classified into three categories:

(a) DDQ in the S1 and S2 solvents:

DDQ behaved similarly in the S1 and S2 solvents. DDQ solubilized in the S1 and S2 created orange-colored solutions that absorbed in UV/Vis region from 285 to 600 nm. The molecule displayed two characteristic bands in the region, one in the UV region (296 nm), and one in the Vis region (350 nm). The one in the UV region was a very strong, narrow band with λ_{max} at 296 nm. The band located in the Vis region was a broad, medium-intensity band with a hill-like shape. This broad band had its λ_{max} at 350 nm with a long tail that ranged from 380 to nearly 600 nm. The intensity of the tail gradually decreased from 380 to 600 nm. In the S1 solvent, this broad band was less intense and had a belly-like or paunch shape; while in the S2 solvent, it was more intense and had a clear hill-like shape. Generally, DDQ absorbed in the same manner in the S1 and S2 solvents but generated a more clearly defined shape in the S2 solvent.

(b) DDQ in the S4 and S5 solvents:

DDQ behaved very similarly in the S4 and S5 solvents. DDQ's dissolution in these two solvents yielded two deep yellow solutions that absorbed in UV/Vis region from 287 to nearly 480 nm. The very strong and narrow band displayed by DDQ in the S1 and S2 solvents also appeared when DDQ was dissolved in the S3 and S4 solvents, but it became narrower, and its λ_{max} blue-shifted from 296 nm in S1 and S2 to 293 nm in the S3 and S4 solvents. Also, the broad band displayed by DDQ in the S1 and S2 solvents also appeared when DDQ was solubilized in the S4 and S5 solvents, but its shape changed from a small hill to a large mountain, and its λ_{max} blue-shifted by ∼10 nm (from 350 nm in S1 and S2 to 339 nm in S4 and S5). The broad band appeared in the S4 and S5 solvents but without the long tail seen in the S1 and S2 solvents.

(c) DDQ in the S3 solvent:

DDQ in the S3 solvent exhibited absorption characteristics that differed from those of the other four solvents. The DDQ-S3 solution had a distinct brown color. The very strong, narrow band observed when DDQ was dissolved in the other solvents broadened in the S3 solvent with an approximate width of 32 nm (from 288 to 320 nm)
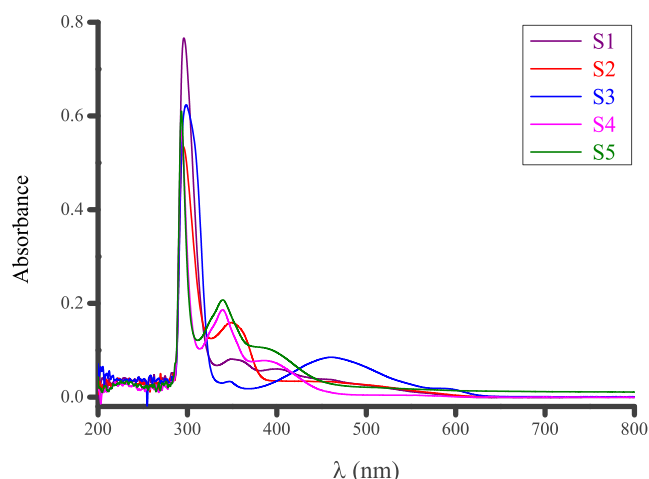

Fig. 3. Color of the DDQ solution in the S1, S2, S3, S4, and S5 solvent (1.0 × 10^{-3} M).

Fig. 4. The UV/Vis spectra of the DDQ acceptor in each solvent (5.0 × 10^{-4} M).

and a λ_{max} at 298 nm. The medium-intensity, broad band at 350 nm when DDQ was dissolved in the S1 and S2 solvents and at 339 nm in the S4 and S5 solvents, became very weak and close to fading when DDQ was dissolved in the S3 solvent. Instead of this band, a new, strong, very broad band appeared at a much longer wavelength. This wide band ranged from 380 to 625 nm and centered at 460 nm. This new broad band, which was not detected when DDQ was dissolved in the S1, S2, S4, or S5 solvents, is the distinguishing band that characterizes the DDQ solution in the S3 solvent. Table 1 summarizes the characteristic absorption bands that appear when the DDQ acceptor was dissolved in the investigated solvents.

3.1.2. CT complexes

Fig. 5 presents the UV/Vis spectra of the HC–DDQ CT complexes in the S1, S2, S3, S4, and S5 solvents, along with that of the free components (HC and DDQ), while Fig. 6 contains those corresponding to the DM–DDQ CT complexes. Generally, the HC and DM molecules behaved similarly when CT complexed with DDQ. This behavior was the same in all solvents, due to the similar chemical structures shared by the HC and DM molecules. This also indicates that the C—F bond present only in the DM molecule does not affect the CT properties between the DM donor and the DDQ. Two categories can be applied to confirm the occurrence of a CT complexation reaction using the UV/Vis spectra of the free donor (D), free acceptor (A), and a mixture between the donor and the acceptor. These categories are:

(a) An increase (with or without broadening) in the intensity of the characteristic absorption band in the UV/Vis spectra of the donor, acceptor, or both.
(b) The formation of a new band in the UV/Vis spectra of the (D + A) system where no measurable absorption was displayed by the free donor and acceptor.

Figs. 5 and 6 indicate that when the HC and DM molecules complexed with the DDQ acceptor, the intensity of the absorption bands of the DDQ accepter was strongly enhanced (Category a). This was the case for all HC–DDQ and DM–DDQ CT complexes prepared in the different solvents. After complexation, the λ_{max} of the DDQ's absorption bands remained at the same position as in the free DDQ or underwent a very slight shift (2–4 nm).

3.2. Bandgap energy

The following equation was used to determine the bandgap energy (E_g):
$(\alpha h\nu)^{1/n} = A (h\nu - E_g)$ where A is a proportionality constant, ν is the light frequency, h is the Plank constant, α is the absorption coefficient, and E_g is the bandgap energy. The exponent (1/n) denotes the nature of the electronic transition, whether indirect or direct and whether forbidden or allowed: n = 3 (indirect, forbidden transitions), n = 3/2 (direct, forbidden transitions), n = 2 (indirect, allowed transitions), and n = 1/2 (direct, allowed transitions). Plots of $h\nu$ (eV) against $(\alpha h\nu)^{1/2}$ for DDQ solubilized in the

investigated solvents (S1, S2, S3, S4, and S5) are given in Fig. 7, while those for the corresponding HC–DDQ and DM–DDQ CT complexes in each solvent are illustrated in Fig. 8. The observed E_g values from these plots are listed in Table 2.

The solution of free DDQ in the S1 solvent had the highest E_g value (3.595 eV) compared with the other solvents, while the DDQ solution in the S3 solvent had the lowest value of E_g (1.625 eV). This outcome indicates that the E_g value of the DDQ acceptor depends strongly on the type of solvent (Fig. 9). The E_g of the DDQ solution in the investigated solvents decreased in the following order: S1 > S2 > S5 > S4 > S3. After DDQ complexed with HC or DM in the S1 and S2 solvents, the value of E_g decreased greatly, approximately by half. In the S3 solvent, the E_g value also decreased but not by as much as in the S1 and S2 solvents. Interestingly, when DDQ interacted with HC or DM in the S4 and S5 solvents, the value of E_g remained unchanged.

3.3. Chn elemental composition

The solid CTCs of the DDQ acceptor with the HC and DM molecules (HC–DDQ and DM–DDQ) were elementally characterized by Perkin-Elmer CHNS Elemental Analyzer (fully automated), and the obtained results in terms of carbon, hydrogen, and nitrogen content (%) are listed in Table 3. The C%, H%, and N% data measured by the instrument aligned with the content values computed theoretically from the molecular formula of the solid CT complexes. The elemental data presented in Table 3 revealed that the stoichiometry of the CT reaction between DDQ and HC or DM in all solvents proceeded at a 1:1 M ratio.

3.4. Hc–DDQ and DM–DDQ stoichiometry

Generally, two methods use UV/Vis absorption spectra to obtain the stoichiometry of a CT complexation, the spectrophotometric titration method and Job's continuous variation method. The HC and DM stoichiometric interactions with the DDQ acceptor were determined in each solvent (S1, S2, S3, S4, or S5) using both methods. Fig. 10 depicts the relative composition of the HC and DM donors with the DDQ acceptor in the five solvents (S1, S2, S3, S4, and S5) determined by the spectrophotometric titration, while the values generated by Job's continuous variation are given in Fig. 11. Both methods suggest that the interaction between each donor (HC and DM) with the DDQ proceeded at a 1:1 M ratio in all of the investigated solvents, as did the solid-state reactions between the donors and DDQ based on the CHN elemental results.

3.5. Determination of formation constant and molar absorptivity

Determining the molar absorptivity (termed as ε_{max}) and the formation constant (termed as K_{CT}) for all of the prepared CT complexes were conducted based on the Benesi–Hildebrand equation (1:1) (Eq. (1)) [111]:

$$(C_a C_d)/A = 1/K_{CT}\varepsilon_{max} + (C_a + C_d)/\varepsilon_{max} \qquad (1)$$

Table 1
Characteristic UV/Vis absorption bands (nm) of the free DDQ acceptor in the investigated and the corresponding CT complex.

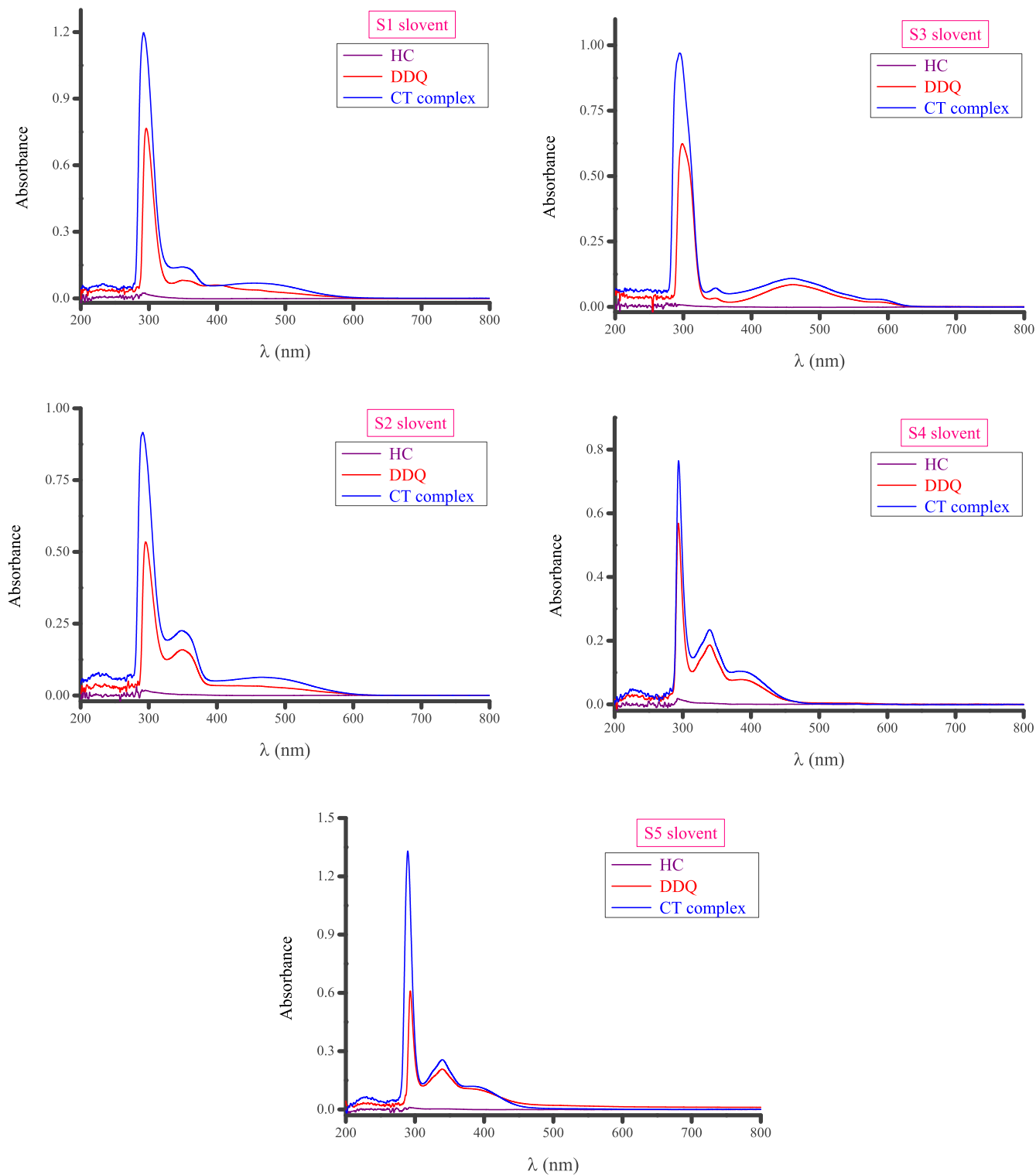| Compound	Characteristic absorption bands (nm)					
	UV			Vis		
	S1, S2	S4, S5	S3	S1, S2	S4, S5	S3
DDQ acceptor	296	293	298	350	339	460
HC–DDQ complex	292	294	295	350	340	460
DM–DDQ complex	297	295	297	348	340	460

Fig. 5. The UV/Vis spectra of the HC–DDQ CT complexes in each solvent (S1, S2, S3, S4, and S5) along with their components (at concentration of 5×10^{-4} M).

In this equation, A is the absorbance of the CT band, and $C_a C_a$ and $C_d C_d$ are the initial concentrations of the acceptor and donor molecules, respectively. In a graphical representation of Eq. (1), plotting the values of $(C_a C_d)/A$ $C_a C_d/A$ versus the values of $(C_a + C_d)$ generates a straight line for which $1/\varepsilon_{max}$ is the slope and $1/K_{CT}$ ε_{max} the intercept. Figs. 12 and 13 contain the Benesi–Hildebrand diagram for the HC–DDQ and DM–DDQ interactions in various solvents, respectively. The derived K_{CT} and ε_{max} values for all of the

prepared CT complexes are listed in Table 4. Data in Table 4 support that the CT complexes of HC and DM with DDQ showed the highest K_{CT} and ε_{max} in the S4 and S5 solvents (non-polar solvents).

3.6. Determination of transition dipole moment and oscillator strength

The transition dipole moment and the oscillator strength have been investigated for all of the prepared CT complexes in various
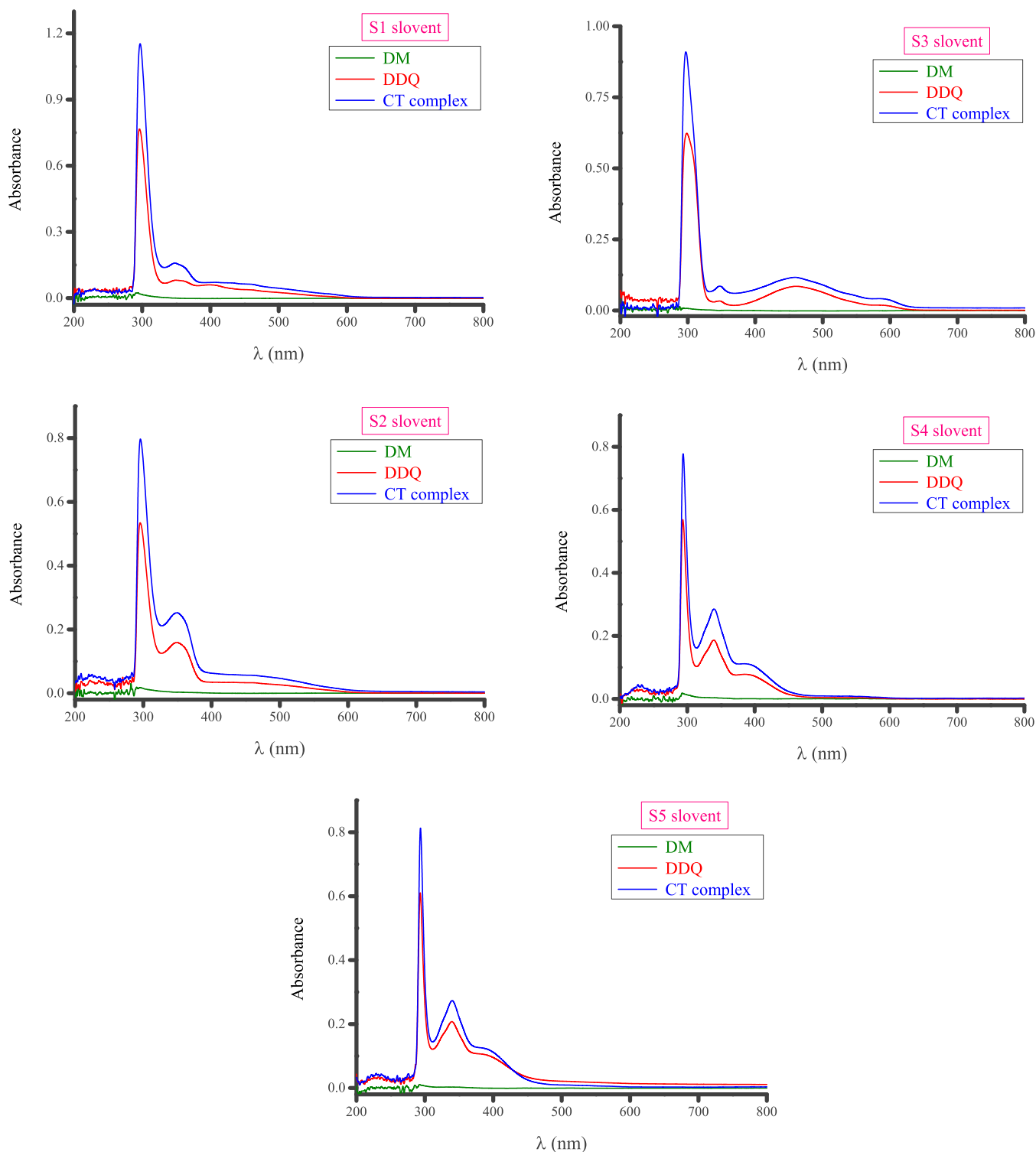
Fig. 6. The UV/Vis spectra of the DM–DDQ CT complexes in each solvent (S1, S2, S3, S4, and S5) along with their components.

solvents to understand the CT characteristics from the donor (HC or DM) to the acceptor (DDQ). The oscillator strength (termed as *f*) is a dimensionless quantity that expresses the transition probability of the band. It states that during the adsorption to emission process in a molecule or atom, the possibility of several electromagnetic radiation transitions from the ground state to the excited state in energy levels exists. The value *f* can be derived using Eq. (2) [112]:

$$f = 4.32^{'} 10^{-9} \varepsilon_{max} n_{1/2} \qquad (2)$$

In this equation, $v_{\frac{1}{2}}$ is the full-width at half-maximum (FWHM) in cm^{-1}. The transition dipole moment (μ_{eg}, in Debye), which used to estimate whether a particular transition is allowed regarding the transient dipole moment induced in the molecule during the transition from a bonding π orbital to an antibonding π^* orbital. μ_{eg} assesses the possibility of radiative transition in a molecule
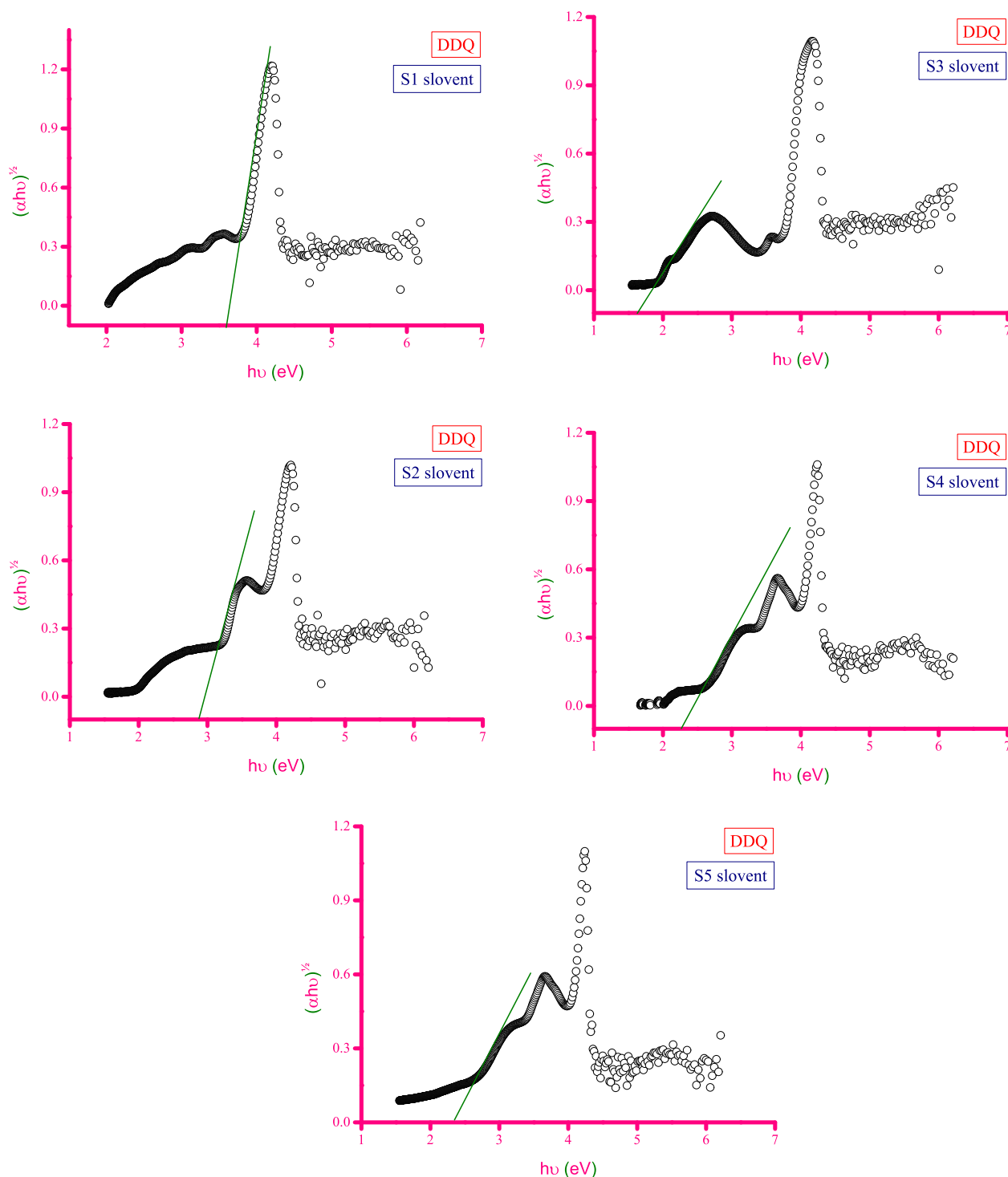
Fig. 7. Plotting the $h\nu$ (eV) versus $(\alpha h\nu)^{\frac{1}{2}}$ for the DDQ acceptor in the investigated solvents (S1, S2, S3, S4, and S5).

from the initial to final states in various solvents. μ_{eg} can be calculated by an equation derived by Tsubumora and Lang [113] (Eq. (3)):

$$m_{eg}^2 = f/(4.32^{'}10^{-7^{'}}n) \tag{3}$$

In this equation, ν is the wavenumber in cm^{-1}. From the data listed in Table 4, the CT complexes of HC and DM with DDQ created

high values of f and μ_{eg} in the S4 and S5 solvent (non-polar solvents). The high values of f and μ_{eg} suggest a strong interaction between the HC–DDQ and DM–DDQ pairs in the S3 and S4 solvents, respectively, with relatively high probabilities for CT transitions. A very strong linear relationship exists between the f and μ values (r = 0.9991 for HC complexes; r = 0.9963 for DM complexes) (Fig. 14). This strong, positive correlation suggests that the f values of the CT complexes in liquid-state increased as their μ_{eg} values increased.
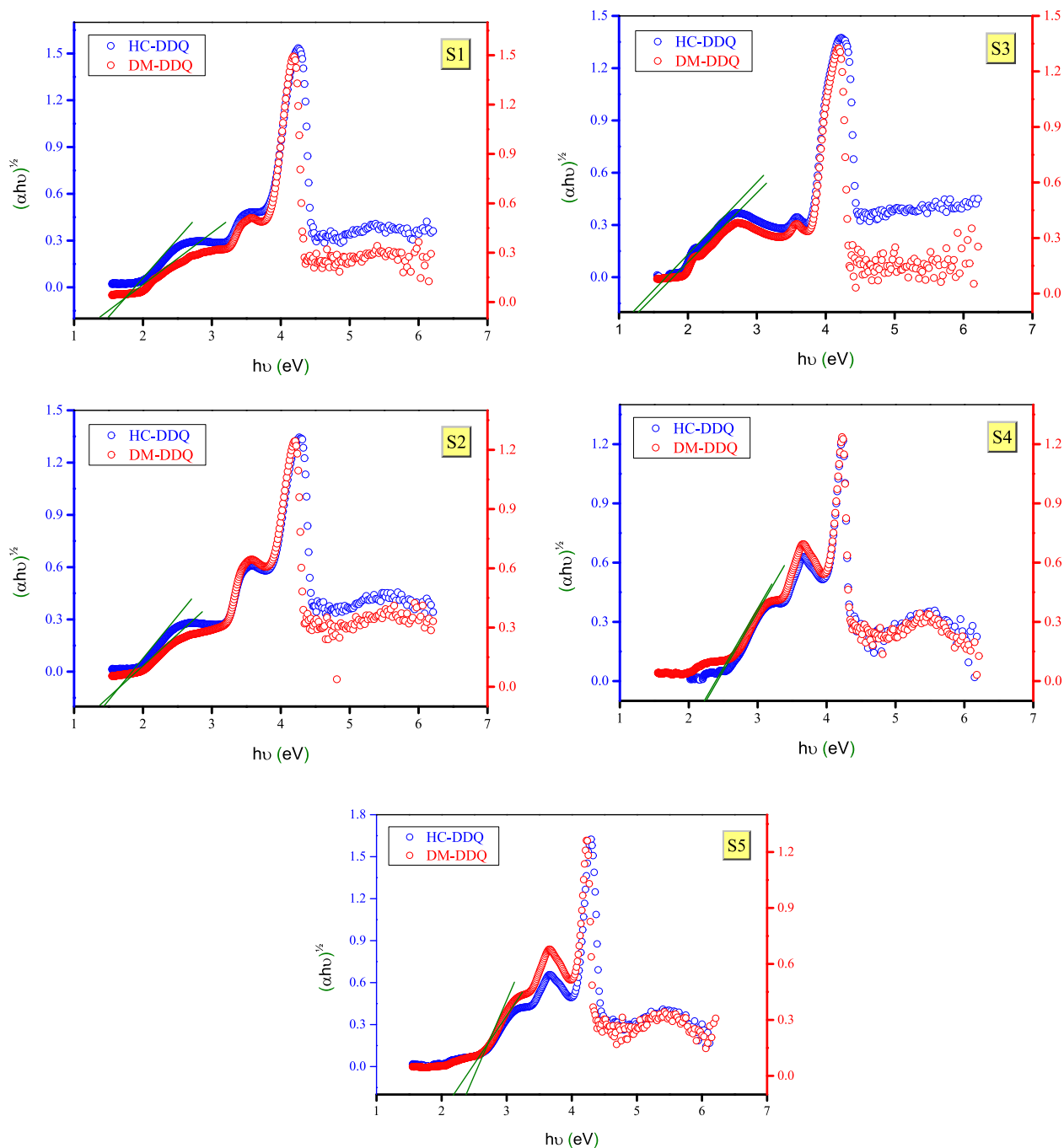
Fig. 8. Plotting the $h\nu$ (eV) versus $(\alpha h\nu)^{1/2}$ for the HC–DDQ and DM–DDQ CT complexes in the investigated solvents.

Table 2
Values of E_g for DDQ alone and its CT complexes in the investigated solvents determined from Tauc's plots.

Compound	E_g (eV)				
	S1	S2	S3	S4	S5
DDQ acceptor	3.595	2.818	1.625	2.264	2.361
HC–DDQ complex	1.508	1.436	1.219	2.276	2.201
DM–DDQ complex	1.376	1.365	1.304	2.230	2.376

3.7. Ft-IR analysis

The FT-IR spectra obtained for the pure HC and DM molecules are presented in Fig. 15a. The characteristic bands of HC were

located at 3414 cm^{-1} ν(O—H), 2920 cm^{-1} [ν(CH$_3$), ν(CH$_2$)], 1704 cm^{-1} ν(C=O) for the carboxylic group, 1642 cm^{-1} ν(C=O) for the carbonyl group, 1434 cm^{-1} δ_{sci}(CH$_3$), 1372 cm^{-1} δ_{rock}(CH$_3$), 1351 cm^{-1} δ_{sci}(CH$_2$), 1277 cm^{-1} δ_{rock}(CH$_2$), 1234 cm^{-1} τ(—CH—C—),
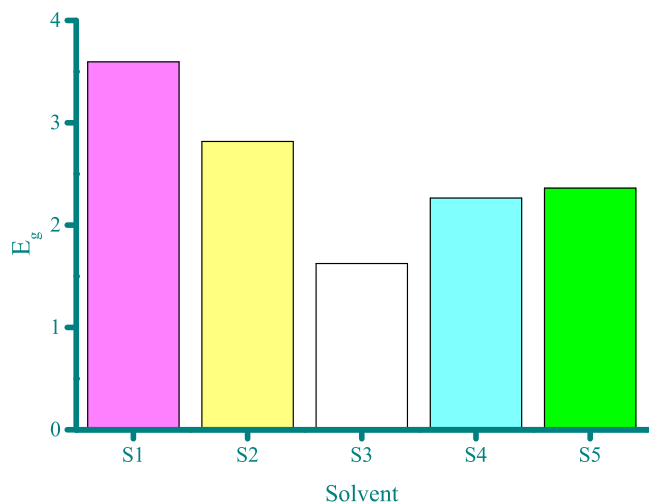
Fig. 9. Value of E$_g$ for DDQ' solution in the investigated solvents.

1106 cm^{-1} ν(C—C), 1041 cm^{-1} (C—O), 936 cm^{-1} [τ(C—C—O—H), δ (O—H) in-plane bending], 891 cm^{-1} [δ$_{wag}$(CH$_3$), δ(C—H) deformation], 779 cm^{-1} δ$_{wag}$(CH$_2$), 636 δ$_{twi}$(CH$_3$), 566 δ$_{twi}$(CH$_2$), and 502 cm^{-1} τ(C—C—C). The absorption spectrum of the DM molecule indicated that the intense characteristic bands of DM appeared at 3393 cm^{-1} ν(O—H), 2946 cm^{-1} [ν(CH$_3$), ν(CH$_2$)], and 1713 cm^{-1} ν (C=O) of the carboxylic group, 1660 and 1618 cm^{-1} ν(C=O) of the carbonyl group, 1543 ν(C=C), 1448 cm^{-1} δ$_{sci}$(CH$_3$), 1403 cm^{-1} δ$_{rock}$(CH$_3$), 1358 cm^{-1} δ$_{sci}$(CH$_2$), 1280 cm^{-1} ν(C—F), 1239 cm^{-1} δ$_{rock}$(CH$_2$), 1207 cm^{-1} τ(—CH—C—), 1127 cm^{-1} ν(C—C), 1054 cm^{-1} (C—O), 984 cm^{-1} [τ(C—C—O—H), δ(O—H) in-plane bending], 897 cm^{-1} [δ$_{wag}$(CH$_3$), δ(C—H) deformation], 855 cm^{-1} τ (C—C—C—H), 761 cm^{-1} δ$_{wag}$(CH$_2$), 690 cm^{-1} [ν(C—C), δ(O—H) out-of-plane bending], 612 δ$_{twi}$(CH$_3$), 536 δ$_{twi}$(CH$_2$), and 482 cm^{-1} τ (C—C—C). [Symbol identification: ν; stretching, δ; bending, τ; torsion, δ$_{sci}$; scissoring, δ$_{wag}$; wagging, δ$_{rock}$; rocking, δ$_{twi}$; twisting].

The characteristic vibrations for the HC and DM molecules were:

(i) O—H vibrations

Both the HC and DM molecules contain three O—H bonds. The three characteristic vibrations of the O—H bond (in-plane and out-of-plane bending, stretching vibrations) resonated at 3414, 936, and 685 cm^{-1}, respectively, in the HC molecule, while the corresponding wavenumbers for the DM molecule were 3393, 984, and 690 cm^{-1}, respectively. The ν(O—H) vibrations appeared in both molecules as a broad, medium to high-intensity band.

(ii) C—F vibrations

Just the DM molecule contained one C—F bond. This bond is the main difference between the structure of DM and HC. In the IR

spectrum of the DM molecule, the ν(C—F) vibrations were observed at 1280 cm^{-1} in accordance with a previous report [114].

(iii) C=O vibrations

Both the HC and DM molecules contain two C=O bonds. One belongs to the carboxylic group and the other to the carbonyl group. The strong band appearing at 1704 cm^{-1} in HC and at 1713 cm^{-1} could be assigned to the ν(C=O) of the carboxylic group. The very strong bands at 1642 cm^{-1} (HC) and 1660 cm^{-1} (DM) conjugated to the —C=O bond of the carbonyl group.

(iv) Methyl and methylene group vibrations

The HC molecule contains eight methylene (CH$_2$) and two methyl (CH$_3$) groups. The DM molecule has five methylene (CH$_2$) and three methyl (CH$_3$) groups. Both molecules displayed a broad absorption band with a medium-intensity center at 2920 cm^{-1} for HC and at 2946 cm^{-1} for DM. The asymmetric and symmetric stretching modes of the CH$_3$ and CH$_2$ groups absorb around this area and, because HC and DM have multiple CH$_3$ and CH$_2$ groups, this band was broad in the spectra of both molecules. The CH$_3$ groups gave rise to four bending vibrational modes: δ$_{sci}$(CH$_3$), δ$_{rock}$(CH$_3$), δ$_{wag}$(CH$_3$), and δ$_{twi}$(CH$_3$). These appeared at 1434, 1372, 890, and 636 cm^{-1}, respectively, for the HC molecule and at 1448, 1403, 897, and 612 cm^{-1}, respectively, for the DM molecule. The CH$_2$ groups in the HC absorbed at 1351, 1277, 779, and 566 cm^{-1} due to the bending vibrations of —CH$_2$: δ$_{sci}$(CH$_2$), δ$_{rock}$(-CH$_2$), δ$_{wag}$(CH$_2$), and δ$_{twi}$(CH$_2$), respectively; the corresponding wavenumbers for the DM molecule were 1358, 1239, 761, and 536 cm^{-1}, respectively [115,116].

(v) C—O vibrations

The stretching vibration of the C—O bond was identified as a very strong band at 1041 cm^{-1} (HC) and 1054 cm^{-1} (DM).

From the FT-IR spectrum of free DDQ (Fig. 15b), the detected bands were 2238, 1675, 1557, 1171, and (893, 798, 720) cm^{-1}, which corresponds to the ν(C≡N), ν(C=O), ν(C=C), δ(C—C), and ν(C—Cl) vibrations, respectively. The DDQ molecule has three different types of electron-withdrawing groups: two cyano groups, two carbonyl groups, and two chloro groups. All of these withdrawing groups take electrons from the aromatic ring of the DDQ molecule, thereby decreasing the electron density of the aromatic ring and increasing the aromatic ring's need for electrons. This situation makes the DDQ molecule a strong electron-deficient unit. When the DDQ acceptor interacted with the HC or DM molecules, it accepted an electronic charge from the donating sites of the HC or DM molecules [117–121]. This charge transfer from the donors (HC and DM) to the acceptor (DDQ), (HC → DDQ; DM → DDQ) affects all of the characteristic IR absorption bands of the free donors as well as that of the free acceptor, as seen in the FT-IR spectra of the HC–DDQ and DM–DDQ CT complexes prepared in

Table 3
CHN elemental results of the HC–DDQ and DM–DDQ CT complexes prepared in the S1, S2, S3, S4, and S5 solvents.

Solvent	HC–DDQ complex						DM–DDQ complex					
	C%		H%		N%		C%		H%		N%	
	Calc.	Obtained	Calc.	Obtained	Calc.	Obtained	Calc.	Obtained	Calc.	Obtained	Calc.	Obtained
S1	59.04	59.15	5.09	5.31	4.75	4.64	58.12	57.95	4.68	4.84	4.52	4.75
S2	59.04	58.93	5.09	5.30	4.75	4.85	58.12	57.91	4.68	4.55	4.52	4.70
S3	59.04	58.91	5.09	4.95	4.75	4.66	58.12	58.03	4.68	4.79	4.52	4.72
S4	59.04	59.16	5.09	5.28	4.75	4.70	58.12	58.35	4.68	4.57	4.52	4.34
S5	59.04	59.10	5.09	4.97	4.75	4.88	58.12	58.26	4.68	4.53	4.52	4.38

Fig. 10. The composition of donors (HC or DM) and DDQ in different solvents (S1, S2, S3, S4, and S5) established by the spectrophotometric titration method.

various solvents (S1, S2, S3, S4, and S5) presented in Figs. 16a and 16b. The band resulting from the C≡N stretching vibrations of the DDQ acceptor shifted from 2238 cm^{-1} to a lower frequency around ∼2225 cm^{-1} in the CT complexes with HC and to ∼2232 cm^{-1} in the CT complexes with DM. The bands belonging to the ν(C=O) in the free HC molecule were affected in their position and inten-

sity after complexation with DDQ. They shifted from 1704 and 1642 cm^{-1} in the free HC molecule to around ∼1717 and ∼1615 cm^{-1} in the HC–DDQ complexes. The same was observed for the DM–DDQ complexes, the bands were shifted from 1713 and 1660 cm^{-1} in the free DM sample to around ∼1698 and ∼1675 cm^{-1} in the DM–DDQ complexes.
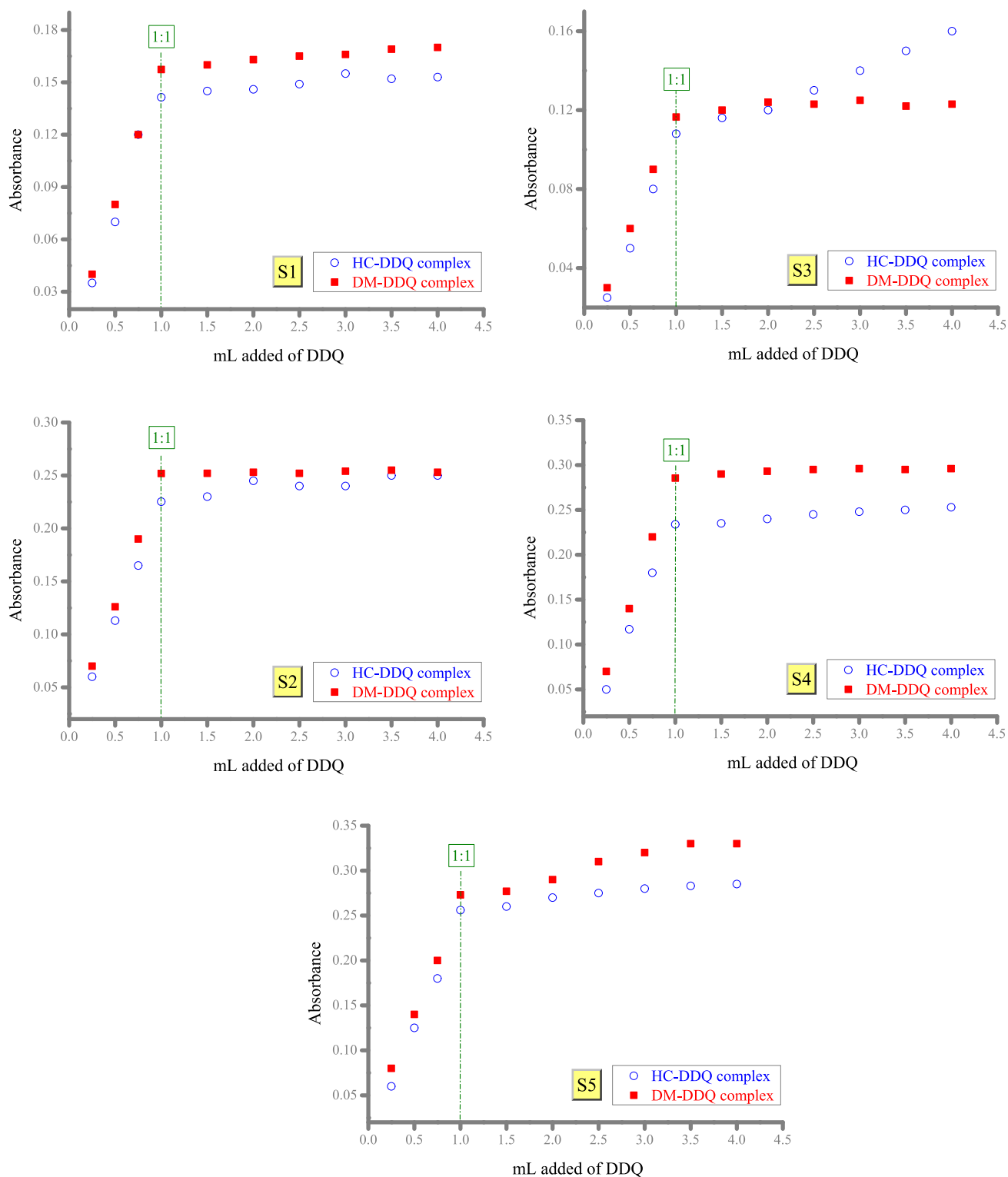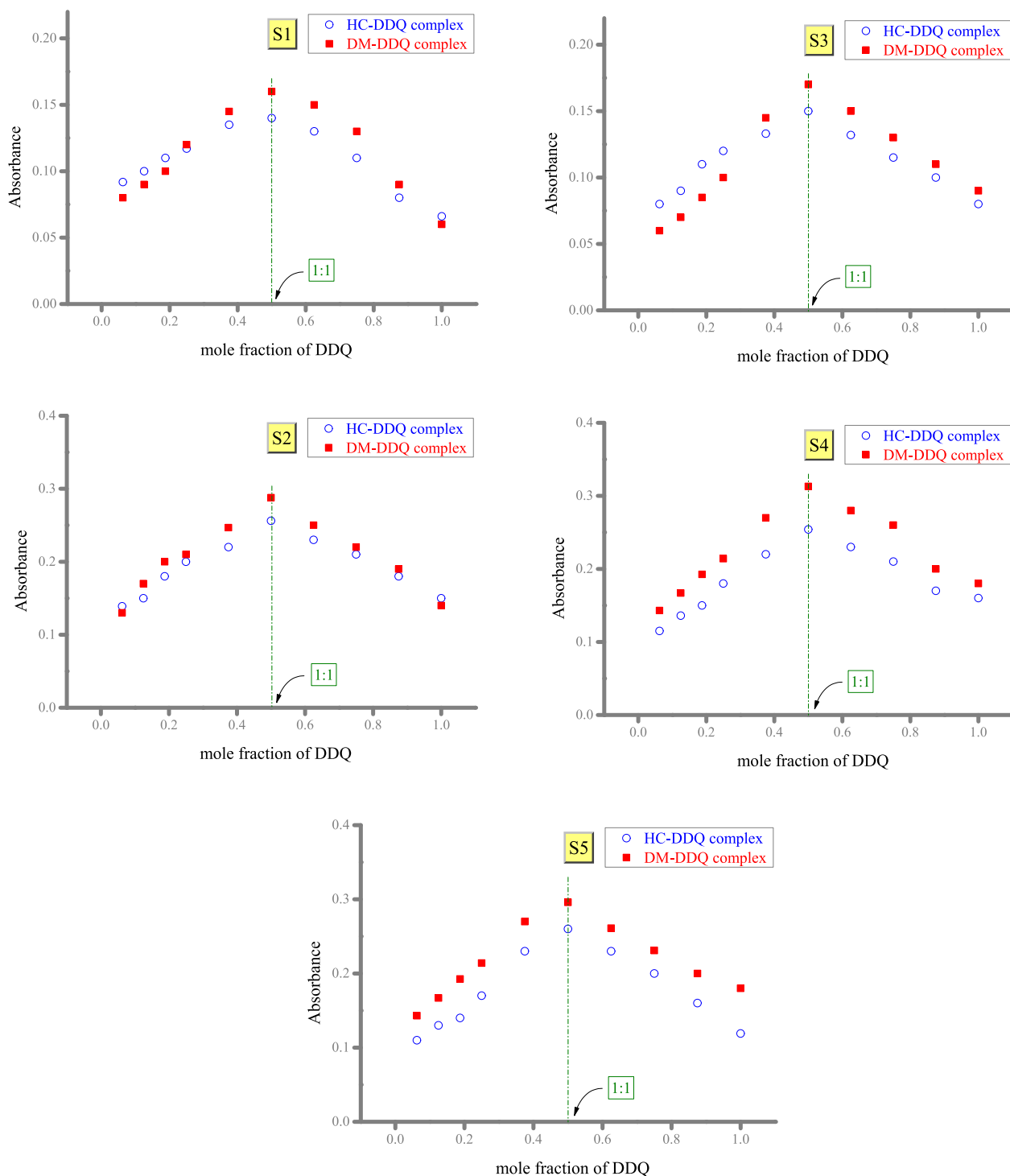
Fig. 11. The composition of donors (HC or DM) and DDQ in different solvents (S1, S2, S3, S4, and S5) established by the Job's continuous variation method.

4. Conclusions

COVID-19 is an ongoing and relapsing epidemiologic phenomenon. This work represents our contribution to the global efforts to stop the spread of the COVID-19 pandemic and the associated economic, medical, and psychological costs by obtaining a vaccine or cure for this disease. Providing new insight into the CT properties of pharmacologically effective drugs used to combat

the COVID-19 pandemic could help researchers alike to develop the treatments and vaccines. Several drugs have been tested, and one class of drugs has received considerable attention, corticosteroids. Two drugs of this class are widely used as adjunctive therapies in the treatment of COVID-19, hydrocortisone (HC) and dexamethasone (DM). Herrin, we prepared 10 CT complexes of HC and DM molecules with the DDQ acceptor. The CT complexes were prepared in five different solvents (S1, S2, S3, S4, and S5).

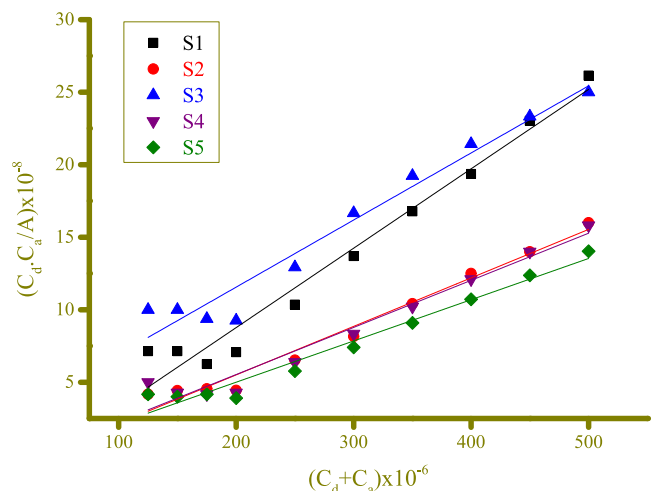**Fig. 12.** The Benesi-Hildebrand diagram for the HC donor and DDQ interaction in various solvents.
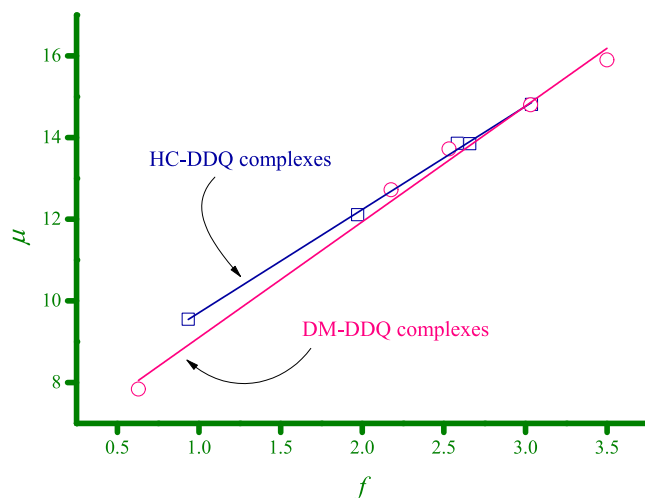

Fig. 14. Linear correlation between transition dipole moment (μ_{eg}) and oscillator strength (f).
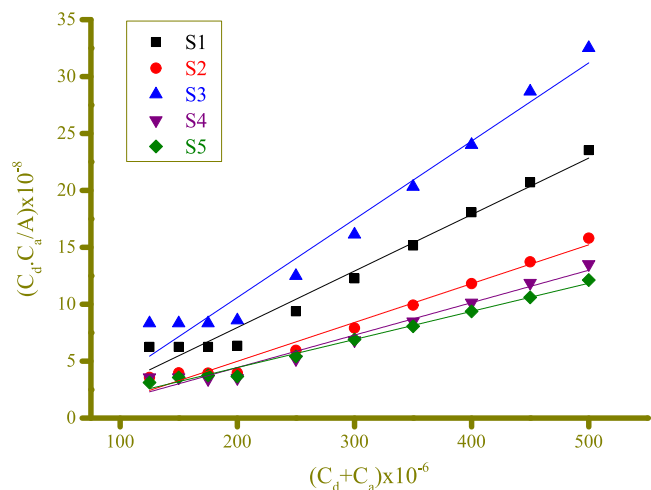
Fig. 13. The Benesi-Hildebrand diagram for the DM donor and DDQ interaction in various solvents.
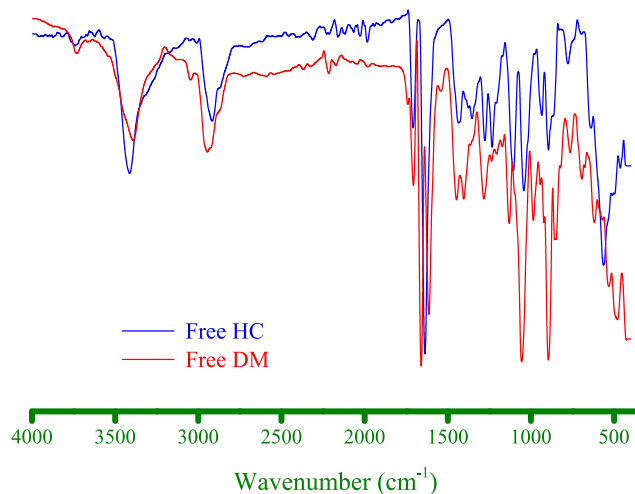
Fig. 15a. IR spectra of free the donors (HC and DM).

Table 4
The formation constant (K_{CT}), molar extinction coefficient (ε_{max}), oscillator strength (f), and dipole moment (μ) for the HC–DDQ and DM–DDQ CT complexes according to solvent type.

Solvent	HC–DDQ CT complexes					DM–DDQ CT complexes				
	λ_{max} (nm)	K_{CT} (L mol^{-1})	ε_{max} (L mol^{-1} cm^{-1})	f –	μ (Debye)	λ_{max} (nm)	K_{CT} (L mol^{-1})	ε_{max} (L mol^{-1} cm^{-1})	f –	μ (Debye)
S1	350	25.1×10^5	18.26×10^4	1.972	12.11	350	25.2×10^5	20.16×10^4	2.177	12.72
S2	350	28.3×10^5	29.90×10^4	2.583	13.86	350	18.6×10^5	29.32×10^4	2.532	13.72
S3	460	20.0×10^5	21.62×10^4	0.934	9.55	460	21.8×10^5	14.55×10^4	0.629	7.84
S4	340	33.6×10^5	30.77×10^4	2.659	13.85	340	32.5×10^5	35.08×10^4	3.031	14.80
S5	340	41.5×10^5	35.16×10^4	3.037	14.81	340	49.2×10^5	40.50×10^4	3.499	15.9

Fig. 15b. IR spectrum of the free DDQ acceptor.

Fig. 16a. IR spectra of the HC–DDQ complexes prepared in various solvents.

Fig. 16b. IR spectra of the DM–DDQ complexes prepared in various solvents.

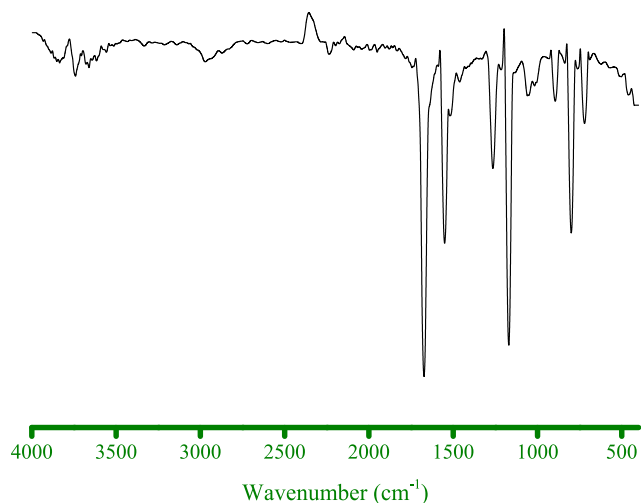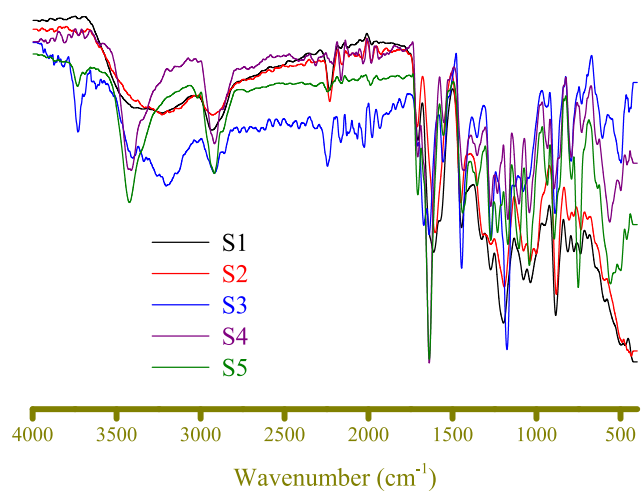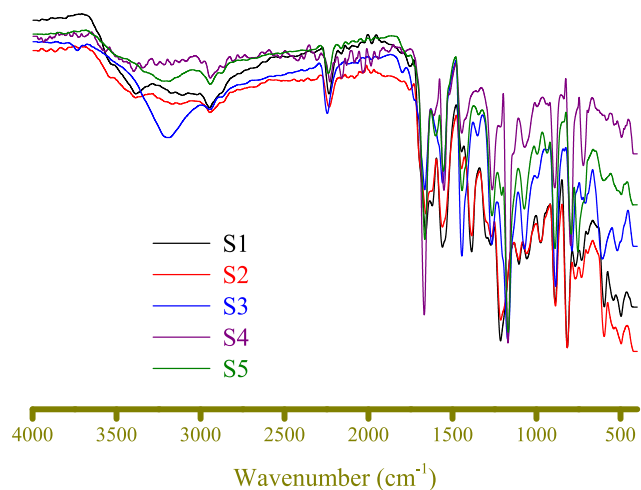Both molecules behaved similarly when complexed with DDQ in each solvent. We found that both HC and DM strongly complexed with DDQ in the S4 and S5 solvents.

CRediT authorship contribution statement

Abdel Majid A. Adam: Data curation, Funding acquisition, Project administration, Writing – original draft, Writing – review & editing. **Hosam A. Saad::** Supervision, Conceptualization, Software, Validation, Visualization. **Moamen S. Refat:** Supervision, Conceptualization, Software, Validation, Visualization. **Mohamed S. Hegab:** Investigation, Formal analysis, Methodology, Resources.

Declaration of Competing Interest

The authors declare that they have no known competing financial interests or personal relationships that could have appeared to influence the work reported in this paper.

Acknowledgements

References

[1] J. Andreani, M. Le Bideau, I. Duflot, P. Jardot, C. Rolland, M. Boxberger, N. Wurtz, J. Rolain, P. Colson, B. La Scola, D. Raoult, *In vitro* testing of combined hydroxychloroquine and azithromycin on SARS-CoV-2 shows synergistic effect, Microb. Pathog. 145 (2020) 104228.

[2] N. Zhu, D. Zhang, W. Wang, X. Li, B. Yang, J. Song, X. Zhao, B. Huang, W. Shi, R. Lu, P. Niu, F. Zhan, X. Ma, D. Wang, W. Xu, G. Wu, G.F. Gao, D. Phil. W. Tan, A novel coronavirus from patients with pneumonia in China, 2019, N. Engl. J. Med. 382 (2020) 727–733.

[3] Organization WH, WHO director-General's opening remarks at the media briefing on COVID-19, 11 March 2020, Geneva, Switzerland, 2020.

[4] L. Pasin, P. Navalesi, A. Zangrillo, A. Kuzovlev, V. Likhvantsev, L.A. Hajjar, S. Fresilli, M.V.G. Lacerda, G. Landoni, Corticosteroids for patients with coronavirus disease 2019 (COVID-19) with different disease severity: a meta-analysis of randomized clinical trials, J. Cardiothorac. Vasc. Anesth. 35 (2) (2021) 578–584.

[5] Johns Hopkins Coronavirus Resource Center, COVID-19 Data in Motion, Accessed August 30, 2021. <https://coronavirus.jhu.edu>.

[6] M. Alkotaji, Azithromycin and ambroxol as potential pharmacotherapy for SARS-CoV-2, Int. J. Antimicrob. Agents 56 (6) (2020) 106192.

[7] Y. Zheng, J. Shang, Y. Yang, C. Liu, Y. Wan, Q. Geng, M. Wang, R. Baric, F. Li, Lysosomal proteases are a determinant of coronavirus tropism, J. Virol 92 (2018) e01504–e1518.

[8] D. Annane, Corticosteroids for COVID-19, J. Intens. Med. 1 (2021) 14–25.

[9] M.A. Gonzalez-Moles, P. Morales, A. Rodriguez-Archilla, I.R. Isabel, S. Gonzalez-Moles, Treatment of severe chronic oral erosive lesions with clobetasol propionate in aqueous solution, Oral Surg. Oral Med. Oral Pathol. Oral Radiol. Endod. 93 (3) (2002) 264–270.

[10] M. Kosaka, Y. Yamazaki, T. Maruno, K. Sakaguchi, S. Sawaki, Corticosteroids as adjunctive therapy in the treatment of coronavirus disease, A report of two cases and literature review, J. Infect. Chemother. 27 (2021) (2019) 94–98.

[11] A.K. Singh, A. Majumdar, R. Singh, A. Misra, D. Metab, Syndr.: Clin. Res. Rev. 14 (2020) 971–978.

[12] S.C. Sweetman (Ed.), Martindale: The Complete Drug Reference, 37th ed., Pharmaceutical Press, London, England, UK, 2011.

[13] E.J. Cano, X.F. Fuentes, C.C. Campioli, J.C. O'Horo, O.A. Saleh, Y. Odeyemi, H. Yadav, Z. Temesgen, Impact of corticosteroids in coronavirus disease 2019 outcomes, CHEST 159 (3) (2021) 1019–1040.

[14] R. Huang, C. Zhu, J. Wang, L. Xue, C. Li, X. Yan, S. Huange, B. Zhang, L. Zhu, T. Xu, F. Ming, Y. Zhao, J. Cheng, H. Shao, X. Zhao, D. Sang, H. Zhao, X. Guan, X. Chen, Y. Chen, J. Wei, R. Issa, L. Liu, X. Yan, C. Wu, Corticosteroid therapy is associated with the delay of SARS-CoV-2 clearance in COVID-19 patients, Euro. J. Pharmacol. 889 (2020) 173556.

[15] K. Chatterjee, C. Wu, A. Bhardwaj, M. Siuba, Steroids in COVID-19: an overview, Cleve. Clin. J. Med. 20 (Aug 2020), https://doi.org/10.3949/ccjm.87a.ccc059.

[16] N. Sharma, A.S. Reddy, K. Yun, Chemosphere 282 (2021) 131029.

[17] C. Liu, Z. Zhou, G. Liu, Q. Wang, J. Chen, L. Wang, Y. Zhou, G. Dong, X. Xu, Y. Wang, Y. Guo, M. Lin, L. Wu, G. Du, C. Wei, X. Zeng, X. Wang, J. Wu, H. Zhou,

Efficacy and safety of dexamethasone ointment on recurrent aphthous ulceration, Am. J. Med. 125 (3) (2012) 292–301.

[18] K. Allen, Dexamethasone: An all purpose agent?, Austral Anaesth. (2007) 65–70.

[19] A.E. Coutinho, K.E. Chapman, The anti-inflammatory and immunosuppressive effects of glucocorticoids, recent developments and mechanistic insights, Mol. Cell. Endocrinol. 335 (1) (2011) 2–13.

[20] S. Shakya, I.M. Khan, Charge transfer complexes: Emerging and promising colorimetric real-time chemosensors for hazardous materials, J. Hazard. Mater. 403 (2021) 123537.

[21] A.S. Al-Attas, M.M. Habeeb, D.S. Al-Raimi, Spectrophotometric determination of some amino heterocyclic donors through charge transfer complex formation with chloranilic acid in acetonitrile, J. Mol. Liq. 148 (2–3) (2009) 58–66.

[22] J. Seliger, V. Zagar, K. Gotoh, H. Ishida, A. Konnai, D. Amino, T. Asaji, Hydrogen bonding in 1,2-diazine–chloranilic acid (2 : 1) studied by a ^{14}N nuclear quadrupole coupling tensor and multi-temperature X-ray diffraction, Phys. Chem. Chem. Phys. 11 (13) (2009) 2281–2286.

[23] A.S. Gaballa, C. Wagner, S.M. Teleb, E.M. Nour, M.A.F. Elmosallamy, G.N. Kaluderovic, H. Schmidt, D. Steinborn, Preparation, spectroscopic and structural studies on charge-transfer complexes of 2,9-dimethyl-1,10-phenanthroline with some electron acceptors, J. Mol. Struct. 876 (1–3) (2008) 301–307.

[24] R.S. Mulliken, W.B. Person, Molecular Complexes, Wiley, New York, 1969.

[25] R.S. Mulliken, Structures of complexes formed by halogen molecules with aromatic and with oxygenated solvents, J. Am. Chem. Soc. 72 (1950) 600–608.

[26] R. Foster, Organic Charge-Transfer Complexes, Academic Press, London, 1969.

[27] R.S. Mulliken, Molecular compounds and their spectra. III. The interaction of electron donors and acceptors, J. Phys. Chem. 56 (7) (1952) 801–822.

[28] A.M.A. Adam, H.A. Saad, A.A. Atta, M. Alsawat, M.S. Hegab, T.A. Altalhi, M.S. Refat, Utilization of charge-transfer complexation to generate carbon-based nanomaterial for the adsorption of pollutants from contaminated water: Reaction between urea and vacant *orbital* acceptors, J. Mol. Liq. 341 (2021) 117416.

[29] M.S. Refat, H.A. Saad, A.A. Gobouri, M. Alsawat, A.M.A. Adam, S.M. El-Megharbel, Charge transfer complexation between some transition metal ions with azo Schiff base donor as a smart precursor for synthesis of nano oxides: An adsorption efficiency for treatment of Congo red dye in wastewater, J. Mol. Liq. (2021) 117140, https://doi.org/10.1016/j.molliq.2021.117140.

[30] A.M.A. Adam, M.S. Refat, T.A. Altalhi, F.S. Aldawsari, G.H. Al-Hazmi, Liquid- and solid-stae study of charge-transfer (CT) interaction between drug triamterene as a donor and tetracyanoethylene (TCNE) as an acceptor, J. Mol. Liq. 336 (2021) 116261.

[31] A.M.A. Adam, M.S. Refat, T.A. Altalhi, K.S. Alsuhaibani, Charge-transfer complexation of TCNE with azithromycin, the antibiotic used worldwide to treat the coronavirus disease (COVID-19). Part IV: A comparison between solid and liquid interactions, J. Mol. Liq. 340 (2021) 117224.

[32] A.M.A. Adam, H.A. Saad, A.M. Alsuhaibani, M.S. Refat, M.S. Hegab, Charge-transfer chemistry of azithromycin, the antibiotic used worldwide to treat the coronavirus disease (COVID-19). Part III: A green protocol for facile synthesis of complexes with TCNQ, DDQ, and TFQ acceptors, J. Mol. Liq. 335 (2021) 116250.

[33] A.M.A. Adam, H.A. Saad, A.M. Alsuhaibani, M.S. Refat, M.S. Hegab, Charge-transfer chemistry of azithromycin, the antibiotic used worldwide to treat the coronavirus disease (COVID-19). Part II: Complexation with several π-acceptors (PA, CLA, CHL), J. Mol. Liq. 325 (2021) 115121.

[34] A.M.A. Adam, H.A. Saad, A.M. Alsuhaibani, M.S. Refat, M.S. Hegab, Charge-transfer chemistry of azithromycin, the antibiotic used worldwide to treat the coronavirus disease (COVID-19). Part I: Complexation with iodine in different solvents, J. Mol. Liq. 325 (2021) 115187.

[35] A.M.A. Adam, M.S. Refat, T.A. Altalhi, F.S. Aldawsari, Charge-transfer (CT) dynamics of triamterene with 2,3-dichloro-5, 6-dicyano-p-benzoquinone acceptor: A n→π* model CT complex generated by liquid- and solid-state reactions, J. Mol. Liq. 334 (2021) 116119.

[36] A.M.A. Adam, T.A. Altalhi, H.A. Saad, A.M. Alsuhaibani, M.S. Refat, M.S. Hegab, Correlations between spectroscopic data for charge-transfer complexes of two artificial sweeteners, aspartame and neotame, generated with several π-acceptors, J. Mol. Liq. 334 (2021) 115904.

[37] A.M.A. Adam, T.A. Altalhi, H.A. Saad, M.S. Refat, M.S. Hegab, Exploring the charge-transfer chemistry of fluorine-containing pyrazolin-5-ones: The complexation of 1-methyl-3-trifluoromethyl-2-pyrazoline-5-one with five π-acceptors, J. Mol. Liq. 331 (2021) 115814.

[38] A.M.A. Adam, M.S. Refat, A comparison of charge-transfer complexes of iodine with some antibiotics formed through two different approaches (liquid-liquid vs solid-solid), J. Mol. Liq. 329 (2021) 115560.

[39] R.M. Alghanmi, M.T. Basha, S.M. Soliman, R.K. Alsaeedi, Synthesis, and spectroscopic, nanostructure, surface morphology, and density functional theory studies of new charge-transfer complexes of amifampridine with π-acceptors, J. Mol. Liq. 326 (2021) 115199.

[40] X. Luo, W. Shi, Y. Yang, Y. Li, Fluorescence probes detecting O$_2$•⁻ based on intramolecular charge transfer and excited-state intramolecular proton transfer mechanisms, J. Mol. Liq. 322 (2021) 114886.

[41] S. Halder, R. Aggrawal, V.K. Aswal, D. Ray, S.K. Saha, Study of refolding of a denatured protein and microenvironment probed through FRET to a twisted intramolecular charge transfer fluorescent biosensor molecule, J. Mol. Liq. 322 (2021) 114532.

[42] I.M. Khan, K. Alam, M.J. Alam, Exploring charge transfer dynamics and photocatalytic behavior of designed donor-acceptor complex: Characterization, spectrophotometric and theoretical studies (DFT/TD-DFT), J. Mol. Liq. 310 (2020) 113213.

[43] M.T. Basha, R.M. Alghanmi, S.M. Soliman, W.J. Alharby, Synthesis, spectroscopic, thermal, structural characterization and DFT/TD-DFT computational studies for charge transfer complexes of 2,4-diamino pyrimidine with some benzoquinone acceptors, J. Mol. Liq. 309 (2020) 113210.

[44] X. Li, Z. Lai, J. Gu, W. Liu, J. Gao, Q. Wang, Sequential determination of cerium (IV) ion and ascorbic acid via a novel organic framework: A subtle interplay between intramolecular charge transfer (ICT) and aggregated-induced-emission (AIE), J. Mol. Liq. 304 (2020) 112705.

[45] T.A. Altalhi, Utilization of tannic acid into spherical structured carbons based on charge-transfer complexation with tetracyanoethylene acceptor: Liquid-liquid and solid-solid interactions, J. Mol. Liq. 300 (2020) 112325.

[46] A. Karmakar, P. Bandyopadhyay, S. Banerjee, N.C. Mandal, B. Singh, Synthesis, spectroscopic, theoretical and antimicrobial studies on molecular charge-transfer complex of 4-(2-thiazolylazo)resorcinol (TAR) with 3, 5-dinitrosalicylic acid, picric acid, and chloranilic acid, J. Mol. Liq. 299 (2020) 112217.

[47] F.A. Al-Saif, A.A. El-Habeeb, M.S. Refat, H.H. Eldaroti, A.M.A. Adam, H. Fetooh, H.A. Saad, Chemical and physical properties of the charge transfer complexes of domperidone antiemetic agent with π-acceptors, J. Mol. Liq. 293 (2019) 111517.

[48] F.A. Al-Saif, A.A. El-Habeeb, M.S. Refat, A.M.A. Adam, H.A. Saad, A.I. El-Shenawy, H. Fetooh, Characterization of charge transfer products obtained from the reaction of the sedative-hypnotic drug barbital with chloranilic acid, chloranil, TCNQ and DBQ organic acceptors, J. Mol. Liq. 287 (2019) 110981.

[49] H. AlRabiah, H.A. Abdel-Aziz, G.A.E. Mostafa, Charge transfer complexes of brucine with chloranilic acid, 2,3-dichloro-5,6-dicyano-1,4-benzoquinone and tetracyanoquinodimethane: Synthesis, spectroscopic characterization and antimicrobial activity, J. Mol. Liq. 286 (2019) 110754.

[50] S. Khopkar, M. Jachak, G. Shankarling, Viscosity sensitive semisquaraines based on 1, 1, 2-trimethyl-1H-benzo[e]indole: Photophysical properties, intramolecular charge transfer, solvatochromism, electrochemical and DFT study, J. Mol. Liq. 285 (2019) 123–135.

[51] A. Mostafa, S. Madrahimov, J. Fadlallah, S.Y. AlQaradawi, UV–Vis, IR spectra, mass spectrometry and thermal studies of charge transfer complexes formed in the reaction of 1, 4, 8, 11-tetraazacyclotetradecane with π-electron acceptors, J. Mol. Liq. 284 (2019) 616–624.

[52] K.M. Al-Ahmary, M.M. Habeeb, S.H. Aljahdali, Synthesis, spectroscopic studies and DFT/TD-DFT/PCM calculations of molecular structure, spectroscopic characterization and NBO of charge transfer complex between 5-amino-1,3-dimethylpyrazole (5-ADMP) with chloranilic acid (CLA) in different solvents, J. Mol. Liq. 277 (2019) 453–470.

[53] L. Miyan, A. Zulkarnain, Ahmad, Spectroscopic and spectrophotometric studies on hydrogen bonded charge transfer complex of 2-amino-4-methylthiazole with chloranilic acid at different temperatures, J. Mol. Liq. 262 (2018) 514–526.

[54] A.S.A. Almalki, A. Alhadhrami, R.J. Obaid, M.A. Alsharif, A.M.A. Adam, I. Grabchev, M.S. Refat, Preparation of some compounds and study their thermal stability for use in dye sensitized solar cells, J. Mol. Liq. 261 (2018) 565–582.

[55] O.R. Shehab, H. AlRabiah, H.A. Abdel-Aziz, G.A.E. Mostafa, Charge-transfer complexes of cefpodoxime proxetil with chloranilic acid and 2,3-dichloro-5,6-dicyano-1,4-benzoquinone: experimental and theoretical studies, J. Mol. Liq. 257 (2018) 42–51.

[56] R.M. Alghanmi, S.M. Soliman, M.T. Basha, M.M. Habeeb, Electronic spectral studies and DFT computational analysis of hydrogen bonded charge transfer complexes between chloranilic acid and 2,3-dichloro-5,6-dicyano-p-benzoquinone with 2-amino-4-methylbenzothiazole in methanol, J. Mol. Liq. 256 (2018) 433–444.

[57] I.M. Khan, S. Shakya, N. Singh, Preparation, single-crystal investigation and spectrophotometric studies of proton transfer complex of 2,6-diaminopyridine with oxalic acid in various polar solvents, J. Mol. Liq. 250 (2018) 150–161.

[58] A. Karmakar, B. Singh, Charge-transfer complex of 1-(2-Thiazolylazo)-2-naphthol with aromatic nitro compounds: experimental and theoretical studies, J. Mol. Liq. 247 (2017) 425–433.

[59] M. Zhang, M. Zhang, Y. Liu, Y. Chen, K. Zhang, C. Wang, X. Zhao, C. Zhou, J. Gao, X. Xie, D. Zheng, G. Zhao, DFT/TDDFT theoretical investigation on the excited-state intermolecular hydrogen bonding interactions, photoinduced charge transfer, and vibrational spectroscopic properties of deprotonated deoxyadenosine monophosphate [dAMP-H]−anion in aqueous solution: upon photoexcitation of hydrogen-bonded model complexes [dAMP-H]—nH$_2$O (*n* = 0, 1, 2, 3, 4), J. Mol. Liq. 242 (2017) 1118–1122.

[60] A. Karmakar, B. Singh, Charge-transfer interaction of 4-(2-pyridylazo) resorcinol with nitroaromatics: insights from experimental and theoretical result, J. Mol. Liq. 236 (2017) 135–143.

[61] A.S.A. Almalki, A.M. Naglah, M.S. Refat, M.S. Hegab, A.M.A. Adam, M.A. Al-Omar, Liquid and solid-state study of antioxidant quercetin donor and TCNE acceptor interaction: focusing on solvent affect on the morphological properties, J. Mol. Liq. 233 (2017) 292–302.

[62] K.M. Al-Ahmary, S.M. Soliman, R.A. Mekheimer, M.M. Habeeb, M.S. Alenezi, Synthesis, spectral studies and DFT computational analysis of hydrogen

bonded-charge transfer complex between chloranilic acid with 2,4-diamino-quinoline-3-carbonitrile in different polar solvents, J. Mol. Liq. 231 (2017) 602–619.

[63] L. Miyan, S. Qamar, A. Ahmad, Synthesis, characterization and spectrophotometric studies of charge transfer interaction between donor imidazole and π acceptor 2,4-dinitro-1-naphthol in various polar solvents, J. Mol. Liq. 225 (2017) 713–722.

[64] A.M.A. Adam, M.S. Refat, M.S. Hegab, H.A. Saad, Spectrophotometric and thermodynamic studies on the 1:1 charge transfer interaction of several clinically important drugs with tetracyanoethylene in solution-state: part one, J. Mol. Liq. 224 (2016) 311–321.

[65] L. Abdelmalek, M. Fatiha, N. Leila, C. Mouna, M. Nora, K. Djameleddine, Computational study of inclusion complex formation between carvacrol and β-cyclodextrin in vacuum and in water: charge transfer, electronic transitions and NBO analysis, J. Mol. Liq. 224 (2016) 62–71.

[66] K.R. Mahmoud, M.S. Refat, T. Sharshar, A.M.A. Adam, E.A. Manaaa, Synthesis of amino acid iodine charge transfer complexes in situ methanolic medium: chemical and physical investigations, J. Mol. Liq. 222 (2016) 1061–1067.

[67] N. Rahman, S. Sameen, M. Kashif, Spectroscopic study of charge transfer complexation between doxepin and π–acceptors and its application in quantitative analysis, J. Mol. Liq. 222 (2016) 944–952.

[68] N. Singh, I.M. Khan, A. Ahmad, S. Javed, Synthesis, spectrophotometric and thermodynamic studies of charge transfer complex of 5,6-dimethylbenzimidazole with chloranilic acid at various temperatures in acetonitrile and methanol solvents, J. Mol. Liq. 221 (2016) 1111–1120.

[69] K.M. Al-Ahmary, M.S. Alenezi, M.M. Habeeb, Synthesis, spectroscopic and DFT theoretical studies on the hydrogen bonded charge transfer complex of 4-aminoquinoline with chloranilic acid, J. Mol. Liq. 220 (2016) 166–182.

[70] L. Miyan, A. Ahmad, Synthesis, spectroscopic and spectrophotometric studies of charge transfer complex of the donor 3,4-diaminotoluene with π-acceptor 2,3-dichloro-5,6-dicyano-p-benzoquinone in different polar solvents, J. Mol. Liq. 219 (2016) 614–623.

[71] A.M.A. Adam, M.S. Refat, Solution and solid-state investigations of charge transfer complexes caused by the interaction of bathophenanthroline with different organic acceptors in a (methanol + dichloromethane) binary solvent system, J. Mol. Liq. 219 (2016) 377–389.

[72] A.M.A. Adam, M.S. Refat, H.A. Saad, M.S. Hegab, Charge transfer complexation of the anticholinergic drug clidinium bromide and picric acid in different polar solvents: Solvent effect on the spectroscopic and structural morphology properties of the product, J. Mol. Liq. 216 (2016) 192–208.

[73] H.S. El-Sheshtawy, M.M. Ibrahim, M.R.E. Aly, M. El-Kemary, Spectroscopic and structure investigation of the molecular complexes of tris(2-aminoethyl) amine with π-acceptors, J. Mol. Liq. 213 (2016) 82–91.

[74] A.S. Al-Attas, D.S. Al-Raimi, M.M. Habeeb, Spectroscopic analysis, thermodynamic study and molecular modeling of charge transfer complexation between 2-amino-5,6-dimethyl-1,2,4-triazine with DDQ in acetonitrile, J. Mol. Liq. 198 (2014) 114–121.

[75] R. Kumar, A.J.A. Baskar, V. Kannappan, D. RoopSingh, Acoustical and spectroscopic investigation of charge transfer complexes of certain aromatic compounds with iodine in n-hexane at 303 K, J. Mol. Liq. 196 (2014) 404–410.

[76] N. Singh, I.M. Khan, A. Ahmad, S. Javed, Synthesis, crystallographic and spectrophotometric studies of charge transfer complex formed between 2,2′-bipyridine and 3,5-dinitrosalicylic acid, J. Mol. Liq. 191 (2014) 142–150.

[77] R.M. Alghanmi, M.M. Habeeb, Spectral and solvation effect studies on charge transfer complex of 2, 6-diaminopyridine with chloranilic acid, J. Mol. Liq. 181 (2013) 20–28.

[78] R. Kumar, G. Padmanabhan, V. Ulagendran, V. Kannappan, S. Jayakumar, Ultrasonic and optical studies on charge transfer complexes of p-chloranil with certain aromatic hydrocarbons in DMSO at 303.15 K, J. Mol. Liq. 162 (2011) 141–147.

[79] K.M. Al-Ahmary, M.M. Habeeb, E.A. Al-Solmy, Spectroscopic studies of the hydrogen bonded charge transfer complex of 2-aminopyridine with π-acceptor chloranilic acid in different polar solvents, J. Mol. Liq. 162 (2011) 129–134.

[80] V. Ulagendran, R. Kumar, S. Jayakumar, V. Kannappan, Ultrasonic and spectroscopic investigations of charge-transfer complexes in ternary liquid mixtures, J. Mol. Liq. 148 (2–3) (2009) 67–72.

[81] E.H. EL-Mossalamy, Molecular spectroscopic studies of charge transfer complexes of thiourea derivatives with benzoquinones, J. Mol. Liq. 123 (2–3) (2006) 118–123.

[82] A.M.A. Adam, M.S. Hegab, M.S. Refat, H.H. Eldaroti, Proton-transfer and charge-transfer interactions between the antibiotic trimethoprim and several σ- and π- acceptors: a spectroscopic study, J. Mol. Struct. 1231 (2020) 129687.

[83] A.M.A. Adam, H.H. Eldaroti, M.S. Hegab, M.S. Refat, J.Y. Al-Humaidi, H.A. Saad, Measurements and correlations in solution-state for charge transfer products caused from the 1:2 complexation of TCNE acceptor with several important drugs, Spectrochim. Acta A 211 (2019) 166–177.

[84] O.B. Ibrahim, E.A. Manaaa, M.M. AL-Majthoub, A.M. Fallatah, A.M.A. Adam, M.M. Alatibi, J.Y. Al-Humaidi, M.S. Refat, Estimation of metformin drug for the diabetes patients by simple, quick and cheap techniques within the formation of colored charge transfer complexes, Spectrosc. Spect. Anal. 38 (11) (2018) 3622–3630.

[85] M.S. Refat, A.M.A. Adam, M.Y. El-Sayed, Biomarkers charge-transfer complexes of melamine with quinol and picric acid: synthesis,

[86] spectroscopic, thermal, kinetic and biological studies, Arabian J. Chem. 10 (2017) S3482.

[86] A.M.A. Adam, M.S. Refat, H.A. Saad, Quick and simple formation of different nanosized charge-transfer complexes of the antibiotic drug moxifloxacin: an efficient way to remove and utilize discarded antibiotics, C.R. Chim. 18 (2015) 914–928.

[87] A.M.A. Adam, M.S. Refat, H.A. Saad, M.S. Hegab, An environmentally friendly method to remove and utilize the highly toxic strychnine in other products based on proton-transfer complexation, J. Mol. Struct. 1102 (2015) 170–185.

[88] M.S. Refat, A.M.A. Adam, H.A. Saad, Utility of charge-transfer complexation for the assessment of macrocyclic polyethers: spectroscopic, thermal and surface morphology characteristics of two highly crown ethers complexed with acido acceptors, J. Mol. Strutct. 1085 (2015) 178–190.

[89] M.S. Refat, H.A. Saad, A.M.A. Adam, Spectral, thermal and kinetic studies of charge-transfer complexes formed between the highly effective antibiotic drug metronidazole and two types of acceptors: σ- and π-acceptors, Spectrochim. Acta A 141 (2015) 202–210.

[90] M.S. Refat, L.A. Ismail, A.M.A. Adam, Shedding light on the photostability of two intermolecular charge-transfer complexes between highly fluorescent bis-1, 8-naphthalimide dyes and some p-acceptors: a spectroscopic study in solution and solid states, Spectrochim. Acta A 134 (2015) 288–301.

[91] M.S. Refat, H.A. Saad, A.M.A. Adam, H.H. Eldaroti, A structural study of the intermolecular interactions of tyramine with some π-acceptors: quantification of biogenic amines based on charge-transfer complexation, J. Gen. Chem. 85 (1) (2015) 181–191.

[92] M.S. Refat, A.M.A. Adam, H.A. Saad, A.M. Naglah, M.A. Al-Omar, Charge–transfer complexation and photostability characteristics of Iodine with bis-1,8-naphthalimide as a photosensitive biologically active units in solution and in the solid state: linear correlation of photostability and dissociation energy, Int. J. Electrochem. Sci. 10 (2015) 6405–6421.

[93] O.B. Ibrahim, M.M. AL-Majthoub, M.A. Mohamed, A.M.A. Ada, M.S. Refat, Quick and simple formation of charge transfer complexes of brain and nerves phenytoin drug with different π–acceptors: chemical and biological studies, Int. J. Electrochem. Sci. 10 (2015) 1065–1080.

[94] A.M.A. Adam, M.S. Refat, Chemistry of drug interactions: characterization of charge-transfer complexes of Guaifenesin with various acceptors using spectroscopic and thermal methods, J. Gen. Chem. 84 (9) (2014) 1847–1856.

[95] M.S. Refat, H.A. Saad, A.M.A. Adam, Infrared, Raman, ¹H NMR, TG, and SEM Properties of the charge-transfer interactions between Tris(hydroxymethyl) methane with the acceptors picric acid, chloranilic acid, and 1,3-dinitrobenzene, J. Gen. Chem. 84 (7) (2014) 1417–1428.

[96] A.M.A. Adam, Application of charge-transfer complexation for evaluation of the drug-receptor mechanism of interaction: spectroscopic and structure morphological properties of procaine and pilocarpine complexes with chloranilic acid acceptor, J. Gen. Chem. 84 (6) (2014) 1225–1236.

[97] A.M.A. Adam, Nano-structured complexes of reserpine and quinidine drugs with chloranilic acid based on intermolecular H-bond: Spectral and surface morphology studies, Spectrochim. Acta A 127 (2014) 107–114.

[98] M.S. Refat, A.M.A. Adam, T. Sharshar, H.A. Saad, H.H. Eldaroti, Utility of positron annihilation lifetime technique for the assessment of spectroscopic data of some charge-transfer complexes derived from N-(1-Naphthyl) ethylenediamine dihydrochloride, Spectrochim. Acta A 122 (2014) 34–47.

[99] H.H. Eldaroti, S.A. Gadir, M.S. Refat, A.M.A. Adam, Charge-transfer interaction of drug quinidine with quinol, picric acid and DDQ: Spectroscopic characterization and biological activity studies towards understanding the drug–receptor mechanism, J. Pharm. Anal. 4 (2) (2014) 81–95.

[100] M.S. Refat, O.B. Ibrahim, H.A. Saad, A.M.A. Adam, Usefulness of charge–transfer complexation for the assessment of sympathomimetic drugs: spectroscopic properties of drug ephedrine hydrochloride complexed with some p-acceptors, J. Mol. Struct. 1064 (2014) 58–69.

[101] H.H. Eldaroti, S.A. Gadir, M.S. Refat, A.M.A. Adam, Spectroscopic investigations of the charge-transfer interaction between the drug reserpine and different acceptors: towards understanding of drug–receptor mechanism, Spectrochim. Acta A 115 (2013) 309–323.

[102] H.H. Eldaroti, S.A. Gadir, M.S. Refat, A.M.A. Adam, Preparation, spectroscopic and thermal characterization of new charge-transfer complexes of ethidium bromide with π-acceptors. In vitro biological activity studies, Spectrochim. Acta A 109 (2013) 259–271.

[103] A.M.A. Adam, Structural, thermal, morphological and biological studies of proton-transfer complexes formed from 4-aminoantipyrine with quinol and picric acid, Spectrochim. Acta A 104 (2013) 1–13.

[104] A.M.A. Adam, M.S. Refat, H.A. Saad, Spectral, thermal, XRD and SEM studies of charge-transfer complexation of hexamethylenediamine and three types of acceptors: π-, σ- and vacant orbital acceptors that include quinol, picric acid, bromine, iodine, SnCl₄ and ZnCl₂ acceptors, J. Mol. Struct. 1051 (2013) 144–163.

[105] A.M.A. Adam, M.S. Refat, H.A. Saad, Utilization of charge-transfer complexation for the detection of carcinogenic substances in foods: spectroscopic characterization of ethyl carbamate with some traditional π-acceptors, J. Mol. Strut. 1037 (2013) 376–392.

[106] H.H. Eldaroti, S.A. Gadir, M.S. Refat, A.M.A. Adam, Charge transfer complexes of the donor acriflavine and the acceptors quinol, picric acid, TCNQ and DDQ: synthesis, spectroscopic characterizations and antimicrobial studies, Int. J. Electrochem. Sci. 8 (2013) 5774–5800.

[107] A.M.A. Adam, Synthesis, spectroscopic, thermal and antimicrobial investigations of charge-transfer complexes formed from the drug procaine

hydrochloride with quinol, picric acid and TCNQ, J. Mol. Struct. 1030 (2012) 26–39.

[108] A.M.A. Adam, M.S. Refat, T. Sharshar, Z.K. Heiba, Synthesis and characterization of highly conductive charge-transfer complexes using positron annihilation spectroscopy, Spectrochim. Acta A 95 (2012) 458–477.

[109] M.S. Refat, H.A. Saad, A.M.A. Adam, Intermolecular hydrogen bond complexes by in situ charge transfer complexation of o-tolidine with picric and chloranilic acids, Spectrochim. Acta A 79 (2011) 672–679.

[110] M.S. Refat, H.A. Saad, A.M.A. Adam, Proton transfer complexes based on some π-acceptors having acidic protons with 3-amino-6-[2-(2-thienyl)vinyl]-1,2,4-triazin-5(4*H*)-one donor: Synthesis and spectroscopic characterizations, J. Mol. Struct. 995 (1–3) (2011) 116–124.

[111] H.A. Benesi, J.H. Hildebrand, A spectrophotometric investigation of the interaction of iodine with aromatic hydrocarbons, J. Am. Chem. Soc. 71 (8) (1949) 2703–2707.

[112] A.B.P. Lever, Inorganic Electronic Spectroscopy, second ed., Elsevier, Amsterdam, 1985.

[113] H. Tsubumora, R. Lang, Molecular complexes and their spectra. XIII. complexes of iodine with amides, diethyl sulfide and diethyl disulfide, J. Am. Chem. Soc. 83 (9) (1961) 2085–2092.

[114] A. Alagha, A. Nourallah, S. Hariri, Characterization of dexamethasone loaded collagen-chitosan sponge and in vitro release study, J. Drug Deliv. Sci. Technol. 55 (2020) 101449.

[115] A. Sanjana, M.G. Ahmed, J. Gowda BH, Preparation and evaluation of *in-situ* gels containing hydrocortisone for the treatment of aphthous ulcer, J. Oral Biol. Craniofac. Res. 11 (2) (2021) 269–276.

[116] S. Soumya, I. Hubert Joe, A combined experimental and quantum chemical study on molecular structure, spectroscopic properties and biological activity of anti-inflammatory Glucocorticosteroid drug, Dexamethasone, J. Mol. Struct. 1245 (2021) 130999.

[117] A.M.A. Adam, H.A. Saad, A.A. Atta, M. Alsawat, M.S. Hegab, M.S. Refat, T.A. Altalhi, E.H. Alosaimi, A.A.O. Younes, Usefulness of charge-transfer interaction between urea and vacant *orbital* acceptors to generate novel adsorbent material for the adsorption of pesticides from irrigation water, J. Mol. Liq. 349 (2022) 118188.

[118] A.M.A. Adam, M.S. Refat, Analysis of charge-transfer complexes caused by the interaction of the antihypertensive drug valsartan with several acceptors in CH_2Cl_2 and $CHCl_3$ solvents and correlations between their spectroscopic parameters, J. Mol. Liq. 348 (2022) 118466.

[119] A.M.A. Adam, H.A. Saad, M.S. Refat, M.S. Hegab, Charge-transfer complexes of antipsychotic drug sulpiride with inorganic and organic acceptors generated through two different approaches: spectral characterization, J. Mol. Liq. 353 (2022) 118819.

[120] A.M.A. Adam, H.A. Saad, A.A. Atta, M. Alsawat, M.S. Hegab, T.A. Altalhi, M.S. Refat, An environmentally friendly method for removing Hg(II), Pb(II), Cd(II) and Sn(II) heavy metals from wastewater using novel metal–carbon-based composites, Crystals 11 (2021) 882, https://doi.org/10.3390/cryst11080882.

[121] A.M.A. Adam, H.A. Saad, A.A. Atta, M. Alsawat, M.S. Hegab, M.S. Refat, T.A. Altalhi, E.H. Alosaimi, A.A.O. Younes, Preparation and characterization of new CrFeO3-carbon composite using environmentally friendly methods to remove organic dye pollutants from aqueous solutions, Crystals 11 (2021) 960, https://doi.org/10.3390/cryst11080960.